Fast Time-Resolved Magnetic Optical Rotatory Dispersion Measurements. 2. Confirmation of Mueller Analysis and Application to Myoglobin Ligand Photolysis

Raymond M. Esquerra, Robert A. Goldbeck,* Daniel B. Kim-Shapiro,† and David. S. Kliger

Department of Chemistry and Biochemistry, University of California at Santa Cruz, Santa Cruz, California 95064

Received: March 31, 1998; In Final Form: August 28, 1998

Experimental verifications are presented of expressions derived in the preceding paper that describe a simple and sensitive near-null technique for nanosecond time-resolved magnetic optical rotatory dispersion (TRMORD) spectroscopy. Expressions verified include those describing artifacts associated with strain, imperfect Faraday compensation, and photoselection-induced orientation of the sample. The accuracy of MORD data obtained with this method is demonstrated by comparison with MORD curves calculated from the Kramers−Kronig transform of independently measured magnetic circular dichroism (MCD) spectra. The separation of natural and magnetic optical rotations for chiral biological macromolecules and potential artifacts associated with this separation are discussed. This work confirms the prediction in paper 1 in this series that the MORD technique is less sensitive to linear birefringence (arising from strained optics or photoselected samples, for instance) than the related near-null MCD technique previously developed in this lab. Possible problems associated with imperfect Faraday compensation are discussed, as is the prediction in the preceding paper of a coupling between photoselection-induced linear dichroism of the sample and Faraday rotation of the solvent. Photolysis measurements on carbonmonoxymyoglobin demonstrate that an excitation geometry in which the sample is probed along the unique axis of excitation minimizes the latter effect, improving accuracy in MORD measurements on photoselected samples. The TRMORD technique is applied to the ligand rebinding reaction of photolyzed carbonmonoxymyoglobin in Soret-region spectral measurements that demonstrate the ability of this technique to measure multichannel time-resolved magnetooptical data with a precision suitable for global kinetic analysis.

Introduction

Magnetic optical activity (MOA) is a particularly useful spectroscopic tool for studying the structure and electronic configurations of inorganic complexes,[1] porphyrins,[2] heme proteins,[3] and non-heme proteins.[4] The first modern application of magnetic optical rotatory dispersion (MORD) spectroscopy to heme proteins was by Shashoua,[5] who examined the MORD of the oxidized and reduced forms of cytochrome *c* and demonstrated the sensitivity of MORD to the oxidation and ligation states of the heme chromophore. Since then, the MORD of heme proteins has been shown to be sensitive to the redox state, the nature of the axial ligands, the spin state of the iron, and the nature of the protein environment around the chromophore.[6] Magnetic circular dichroism (MCD) largely eclipsed MORD as a probe of MOA chromophores with the advent of modern circular dichroism instruments based on photoelastic modulators and phase-sensitive detection. Nevertheless, the measurement of MORD can have advantages over MCD measurements in some cases, most notably for optically dense samples.

In principle, MORD and MCD contain identical information. Optical activity consists of an absorptive part, circular dichroism (CD), and a dispersive part, circular birefringence (CB) or optical rotatory dispersion (ORD). CD is the differential absorption of left and right circularly polarized light, and CB is the difference in the refractive index of left and right circularly polarized light. The absorptive and dispersive parts of optical activity are related by Kramers−Kronig transforms.[7−9] Natural optical activity (NOA) results from chirality in the structure of a chromophore or its environment. Magnetic optical activity arises from the chirality induced in the motions of charged particles by a magnetic field. It is particularly sensitive to the presence of degeneracies, or near degeneracies, in the electronic structure of a chromophore. As in NOA, MOA has an absorptive part, magnetic circular dichroism, and a dispersive part, magnetic circular birefringence (MCB) (the wavelength dependence of which is proportional to MORD), first observed by Faraday and also known as the Faraday effect.[10] Although they result from different phenomena, NOA and MOA both rotate the plane of polarization of linearly polarized light, their combined effects being additive. MORD is unlike natural ORD, however, in that natural ORD rotates the plane of polarized light in the same sense regardless of the propagation direction, whereas MORD depends on the relative directions of the light propagation and the magnetic field. This difference is used to distinguish the contribution of natural ORD from that of MORD in measurements of total rotation. Quantum mechanical expressions for the magnetic and natural optical activity of perfectly oriented and isotropic samples are available[8,11] and may be derived for partially oriented systems.[12] Expressions for the natural CD and MCD of molecules partially oriented by

* Corresponding author. E-mail: goldbeck@chemistry.ucsc.edu. Fax: (831) 459-2935.

† Present address: Department of Physics, Wake Forest University, Winston-Salem, NC 27109-7507.

10.1021/jp981694p CCC: $15.00
Published on Web 10/14/1998

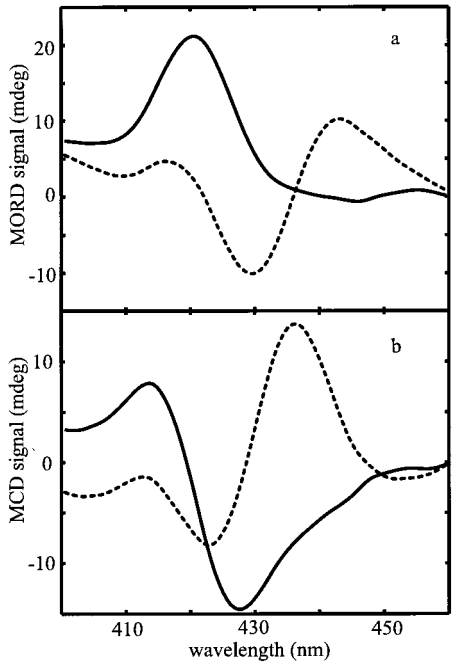

Figure 1. Measured MORD (a) and calculated MCD (b) of MbCO (—) and the 1 μs deoxy photoproduct Mb* (- - -). Sample concentration is 11 μM in a 5-mm path length cell at 26 °C.

photoselection, a case particularly important for time-resolved photolysis experiments, were recently derived.[13,14]

The simple and sensitive technique used in this work to measure nanosecond time-resolved MORD is explained in detail in the preceding paper. This article presents tests of the relationships derived in that paper and an application to the ligand rebinding reaction of photolyzed myoglobin−CO, demonstrating the usefulness of the technique for fast multichannel kinetic spectroscopy.

Experimental Methods

A near-null polarimetric MORD measurement is made by placing the sample between two crossed polarizers and rotating the first polarizer clockwise (looking toward the probe source) and then counterclockwise by a small angle, β, from the crossed position. The measured signal is the ratio of the difference to the sum of the intensities for the clockwise and counterclockwise positions

$$s_D(t) = \frac{I_{+\beta}(t) - I_{-\beta}(t)}{I_{+\beta}(t) + I_{-\beta}(t)} \quad (1)$$

The subscript D denotes the direction of the magnetic field, parallel, P, or antiparallel, A, with respect to the probe propagation direction. The contributions of natural ORD and MORD are separated by taking the difference of the measurements at opposite field directions, that is

$$\mathrm{ORD}(t) = -\beta[s_P(t) + s_A(t)]/4 \quad (2)$$

$$\mathrm{MORD}(t) = -\beta[s_P(t) - s_A(t)]/(4H) \quad (3)$$

where β is in degrees and H is the field strength (T).

Instrument. The TRMORD instrument is the same as the TRORD instrument described previously,[15] except for the addition of a sample magnet and the Faraday compensator. The optical layout is shown in Figure 1 of the preceding paper. A matched pair of electric dipole magnets (GMW Associates, model 3470, Redwood City, CA) provide magnetic fields of 1 T for the sample and the Faraday compensator, which uses a matched cell and buffer solution. A xenon flashlamp produces unpolarized light. The light is polarized by a Glan−Taylor laser polarizer, which is rotated by small angles, $\pm\beta$, from horizontal. A β of 1° is used for the data reported here. The light is then passed through the poles of the magnet (12-mm gap) and enters both the sample and the compensator with a beam diameter of about 7 mm. A frequency doubled (532 nm) Quanta Ray DCR-2A Nd:YAG laser produces 8-ns excitation pulses at 2 Hz. The pulse energy is 12 mJ. A polarizer ensures horizontal polarization of the actinic beam. The collimated probe beam is focused through a 250-mm slit into a Jarrel Ash spectrograph (150 grooves per mm, 450 nm blaze, for the Soret data) and is detected with an EG&G OMA II detector. A Stanford Instruments DG535 delay/pulse generator controls the timing of the detector gate and the firing of the flashlamp with respect to the laser pulse. The pulse timing and optical detection systems are described in more detail elsewhere.[15,16]

The two probe polarizers are oriented along the horizontal (LP1) and vertical (LP2) directions with an accuracy of $\pm 0.013°$.[15] The probe and pump beams propagate at right angles for all of the MORD measurements presented here. The excitation laser is polarized parallel to the probe propagation direction to eliminate any photoselection-induced LB or LD contributions to the kinetic data reported in the last section of the paper. All MCD measurements reported here were obtained with the near-null ellipsometric method.[17] The time-resolved absorption and MCD measurements were performed on instrumentation described previously.[17−20]

Faraday Compensator. Two methods are used in this laboratory to compensate for solvent−cell Faraday rotation with the wavelength dispersion appropriate for multichannel spectral measurements. One approach is to use the natural optical rotation of a chiral substance transparent in the wavelength region under investigation,[19] as the natural and magnetic CBs of materials tend to have very similar dispersions in spectral regions far from the absorption bands. The MORDs of transparent substances, such as water and quartz, obey Verdet's Law[8]

$$[\alpha]_M = V(\lambda)H_D \quad (4)$$

where $[\alpha]_M$ is the molar MORD per unit path length and field intensity, and $V(\lambda)$ is the temperature-dependent Verdet constant for a particular material. $V(\lambda)$ is described by the Drude equation[8]

$$V(\lambda) \approx \sum_j \frac{C_j}{\lambda^2 - \lambda_j^2} \quad (5)$$

where C_j is a constant appropriate to the absorption wavelength, λ_j, and the sum is over all electronic transitions. Equation 5 demonstrates the similarity of the dispersion characteristics of materials far outside absorption bands, where $V(\lambda) \propto \lambda^{-2}$. If parallel and antiparallel field measurements are used to isolate natural ORD from the MORD, a chiral material must be found for each orientation, a condition that is easy to satisfy if both enantiomers are available. However, finding appropriate substances becomes more difficult as wavelengths approach UV absorption bands and the terms in eq 5 begin to diverge. A second, more general method is to use a magnetized solvent blank, i.e., an identical spectral cell containing solvent in a

second magnetic field of equal strength and opposite direction, as a Faraday compensator. The first method was found to work well in the visible spectral region of the heme chromophore but to be less effective for Soret-region MORD measurements, thus all spectra reported here were obtained with the latter method.

Sample Preparation and Data Collection. For measurements intended to test predictions presented in paper 1 of this series, a 10-μM sample of MbCO was prepared in a viscous solvent of 90% glycerol and 10% aqueous sodium phosphate buffer (pH 7.3) by weight. The sample temperature was 26 °C. The glycerol increases the sample viscosity by a factor of 150, which is expected to increase the rotational diffusion time constant from 20 ns to 3 μs.[21] Because orientation disappears through rotational diffusion more slowly at higher viscosities, this is expected to increase the contribution of photoselection-induced linear effects to signals measurable on the current instrument, which has a time resolution of about 100 ns. For the kinetic measurements, myoglobin (Mb) from horse skeletal muscle (Sigma) was diluted with 0.1 mM sodium phosphate buffer, pH 7.3, to give a final concentration of 11 μM. The sample was sealed in a 5-mm path length anaerobic sample cell and reduced anaerobically under 1 atm of CO by addition of sodium dithionite (Fluka) to a final concentration of 2 mM.

Spectra for the glycerol sample in parallel and antiparallel magnet configurations were each collected with 2048 averages. Consequently, each MORD and ORD spectrum consisted of 4096 averages. The data were smoothed using a 15-point (0.6 nm per point) Savitzky−Golay quadratic spectral convolution.

The time-resolved magnetic optical rotatory dispersion TR-MORD (TRORD) measurements for MbCO, dissolved in buffer only, were collected at 10 time delays ranging from 10 μs to 10 ms (3 per decade) after ligand photolysis (512 scans/field direction). The time delay was defined by the interval between the laser photolysis pulse and the center of the 150-ns time gate of the detector. The TRMORD (TRORD) data were smoothed as above and analyzed using singular value decomposition.[22] The decomposed data were then used to determine the lifetime and spectrum associated with exponential decay of the photolyzed sample using a nonlinear least-squares global analysis.[23]

Specific perturbations intentionally imposed on the sample and instrument, such as photoselection, window strain, or incomplete Faraday compensation, are described in the sections pertaining to particular perturbations.

Kramers−Kronig Transforms. In principle, MCD and MCB may be interconverted by use of the following integral transforms:[7−9]

$$\mathrm{MCB}(\nu) = \frac{2\nu^2}{\pi}\int_0^\infty \frac{\mathrm{MCD}(\nu')}{\nu'(\nu'^2-\nu^2)}\,\mathrm{d}\nu' \qquad (6)$$

$$\mathrm{MCD}(\nu) = \frac{-2\nu^3}{\pi}\int_0^\infty \frac{\mathrm{MCB}(\nu')}{\nu'^2(\nu'^2-\nu^2)}\,\mathrm{d}\nu' \qquad (7)$$

Although the integrals in eqs 6 and 7 run over all frequencies, we limited the transform calculations presented below to frequencies within the Soret spectral region (400−480 nm in wavelength space) or within the visible bands (500−650 nm). The Soret bands are intense and, in general, spectrally well separated from the other porphyrin bands (although there is some overlap with the weak N band), so that neglecting these other transitions is not expected to introduce much distortion when transforming between MCD and MCB within the Soret bands. We previously found this approximate transform procedure to work well for the natural Soret CD and CB of hemoglobin.[15] Similarly, the visible bands are the lowest energy porphyrin bands and are well-separated from the next higher energy transitions, the Soret bands. Direct comparisons of the band shapes of measured and transform-calculated MCB presented below for myoglobin show that there, indeed, is reasonable agreement between them in the Soret and visible; distortions within the absorption-band regions for both bands appear to be no greater than several percent. Calculated Soret or visible band TRMCD spectra of greater accuracy could presumably be obtained from limited bandwidth K−K transforms of TRMORD data by extending the range of frequencies in the integration to include neighboring bands.

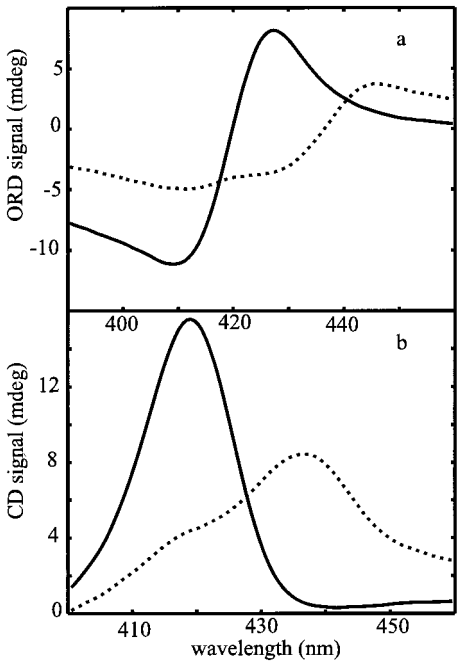

Figure 2. Natural ORD (a) and CD (b) of MbCO (—) and Mb* (- - -), sample as in Figure 1 caption. Note that wavelength regions are different for a and b.

Results and Discussion

Comparison with MCD and CD Measurements. Figure 1 shows the measured MORD spectra of carbonmonoxy and deoxy (1-μs photolysis spectrum) myoglobin and the MCD spectra calculated from the Kramers−Kronig transform (K−K) of the MCB spectra. Figure 2 shows the corresponding ORD and CD spectra. It is known that the absorption spectrum of the 1-μs photolysis intermediate closely resembles a deoxy Mb spectrum.[24] However, there appears to be about a 4−6% contribution by MbCO to the photolyzed spectra shown here. A contribution by MbCO is suggested by the blue shoulder most evident in the CD spectrum in Figure 2b. Consistent with this interpretation is the observation that this feature increases as the photolysis level is decreased by lowering the laser-pulse energy (data not shown). Incomplete photolysis, perhaps from photoselection or geminate recombination, would be the most likely cause of a small (time independent) contribution by MbCO to the 1-μs spectrum.

The Kramers−Kronig transform (K−K) of the Soret MORD spectrum of unphotolyzed MbCO is similar to published MCD spectra measured on conventional instrumentation for sperm whale[25] and with the MCD spectrum measured with the ellipsometric TRMCD apparatus. The 1-μs photolyzed product

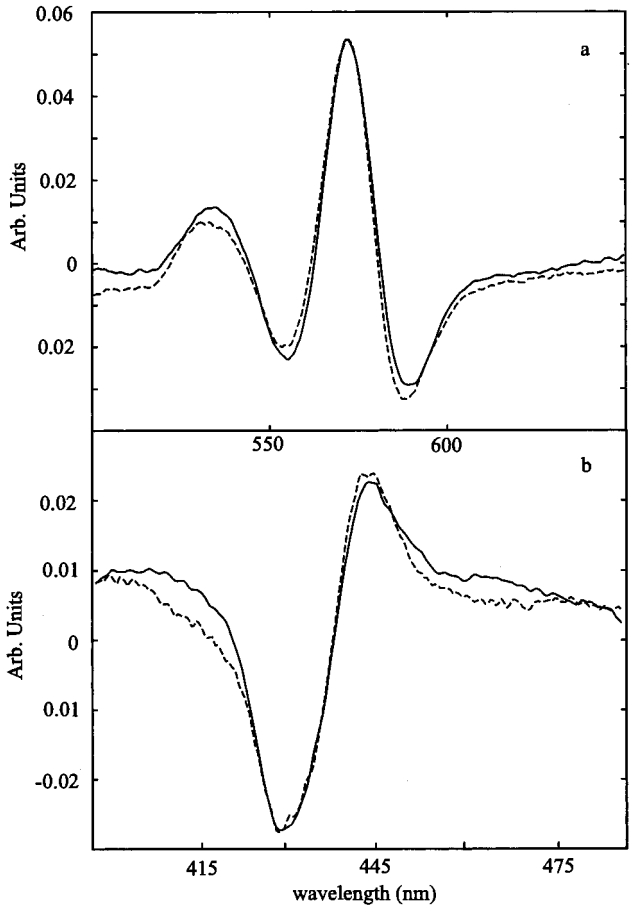

Figure 3. MORD (- - -) and the Kramers−Kronig transform of the MCD (—) of MbCO at 1 μs after photolysis (Mb*): (a) visible bands (concentration 110 μM), (b) Soret bands (concentration 11 μM).

MORD spectrum is similar in intensity and shape to the equilibrium deoxy spectrum of dolphin myoglobin[26,27] and to the K−K transform of the 1-μs MCD spectrum of horse skeletal myoglobin (Figure 3). The comparison in Figure 3 reflects the combined accuracies of the MORD technique and the approximate K−K transform procedure described in the Experimental Methods. The good agreement over both the Soret and visible spectral regions is strong evidence of their separate accuracies, given the unlikelihood of a coincidental cancellation of errors over multiple bands. The unphotolyzed and photolyzed ORD spectra (obtained by summing reversed-field measurements) are similar in intensity and shape to equilibrium MbCO and Mb ORD spectra, and their K−K transforms agree with CD spectra measured on conventional instrumentation.[28]

Application to Biological Molecules. The following three sections address problems that may arise when simultaneously measuring natural and magnetic optical activity in the presence of experimental imperfections such as field drift, imprecise polarizer rotation, and sample degradation. These considerations are particularly pertinent to the application of this new technique for time-resolved MORD measurements to biological macromolecules, which are typically chiral. Note that while the treatment given of the second problem is particular to the near-null technique, the results presented below for field drift and sample degradation are generally applicable to MOA measurements.

Magnetic Field Drift. We first consider the case in which the magnetic-field magnitude differs between the opposed-field measurements. If the fields do not match in magnitude, then the MCB and CB calculated from eq 6 in paper 1 of this series are

$$\mathrm{MCB}_{\mathrm{calc}}(t) = \mathrm{MCB}(t) \tag{8}$$

$$\mathrm{CB}_{\mathrm{calc}}(t) = \mathrm{CB}(t) - \Delta\mathrm{H}\ \mathrm{MCB}(t)/2 \tag{9}$$

where $\Delta H = H_A - H_P$ is the field difference between antiparallel, H_A, and parallel, H_P, configurations, and the average field magnitude, $H_P + {}^1/_2\Delta H$, is used in the denominator of eq 6, paper 1 of this series. Thus, the calculation of MCB is unaffected (eq 8), whereas the calculated CB is distorted by the addition of an MCB component that is proportional to the difference in field strengths (eq 9). If H·MCB and CB are approximately the same size, then typical field mismatches (<1%) will produce a comparably small distortion in observed CB. However, accurately measuring a CB that is small compared to H·MCB puts a proportionately greater demand on field-magnitude stability. The predictions of eqs 8 and 9 are verified in Figure 4 for a particular example, $\Delta H = 0.2$H. In this case, a 20% increase in field strength in the parallel configuration is predicted by eq 9 to introduce a 10% proportion of H·MCB into the CB signal whereas eq 8 predicts no signal distortion from CB in the MCB.

Polarizer Rotation Angle. Similarly, if different βs are used for each field configuration, then

$$\mathrm{MCB}_{\mathrm{calc}}(t) = (\bar{\beta}\cdot\mathrm{MCB}(t) - \Delta\beta\cdot\mathrm{CB}(t)/2H_0)\bar{\beta}/\beta_A\beta_P \tag{10}$$

$$\mathrm{CB}_{\mathrm{calc}}(t) = (\bar{\beta}\cdot\mathrm{CB}(t) - \Delta\beta\cdot H_0\cdot\mathrm{MCB}(t)/2)\bar{\beta}/\beta_A\beta_P \tag{11}$$

where $\bar{\beta}$ and $\Delta\beta$ are, respectively, the average and difference of the measurement angles for the parallel (β_P) and antiparallel (β_A) configurations. The calculated MCB includes a CB term proportional to the difference in reference angles, and, conversely, the calculated CB includes an MCB term. The predictions of eqs 10 and 11 are verified in Figure 4 for a particular example, $\Delta\beta = 0.2\bar{\beta}$.

Sample Degradation. Sample instability and concomitant variation of sample concentration between measurements at different field configurations may be an important consideration in the laser photolysis of biological samples, particularly if limited sample quantity prevents use of a flow system to replace degraded sample. If the effective concentrations for parallel and antiparallel field measurements differ by Δc, then we have

$$\mathrm{MCB}_{\mathrm{calc}}(t) = \overline{\mathrm{MCB}}(t) + (\Delta c/2\bar{c}H)\overline{\mathrm{CB}}(t) \tag{12}$$

$$\mathrm{CB}_{\mathrm{calc}}(t) = \overline{\mathrm{CB}}(t) - (\Delta cH/2\bar{c})\overline{\mathrm{MCB}}(t) \tag{13}$$

where the averages of the magnetic and natural circular birefringence rotations at each configuration are $\overline{\mathrm{MCB}}(t)$ and $\overline{\mathrm{CB}}(t)$, respectively, $\Delta c = c_P - c_A$, and $\bar{c}$ is the average concentration. Note that these equations contain some simplifying assumptions (specifically, neglect of any signal from the photodegradation products and neglect of any change in effective concentration between I_+ and I_- measurements made at a given field configuration), but they nonetheless serve to show that concentration instability tends to mix the MCB and CB signals. (With regard to sample instability within measurements at a given field configuration, it can be shown, starting from eq 5 in ref 15 for instance, that a change in sample transmission ΔT between I_+ and I_- measurements will distort the measured signal by adding a term $\Delta T/2T$, where T is the average transmission.) An example of eqs 12 and 13 is illustrated in Figure 5.

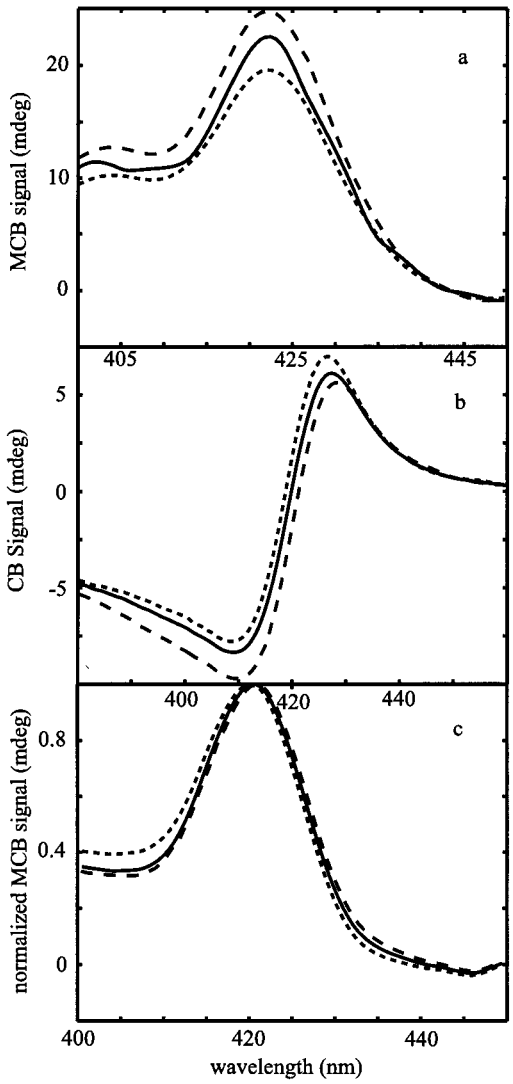

Figure 4. Effects of mismatched rotation angles, $\beta_{P,A}$ (angle mismatch, AM), and field strengths (field mismatch, FM) on the determination of MCB and CB from reverse field measurements (see eqs 8−11 in text). No mismatch (—); FM, magnetic field 20% larger in parallel field configuration (- - -); AM, β 20% larger in parallel configuration (···). (a) MCB. Observed spectrum is increased in amplitude in the FM case, whereas in the AM case, it is distorted by the addition of a −CB component and attenuated. (b) CB. Observed spectrum is distorted by the addition of MCB in the FM case and is distorted by addition of −MCB and attenuated in the AM case. (c) MCB from panel a normalized to maximum intensity to demonstrate distortion of band shape present in AM case, absent in FM case.

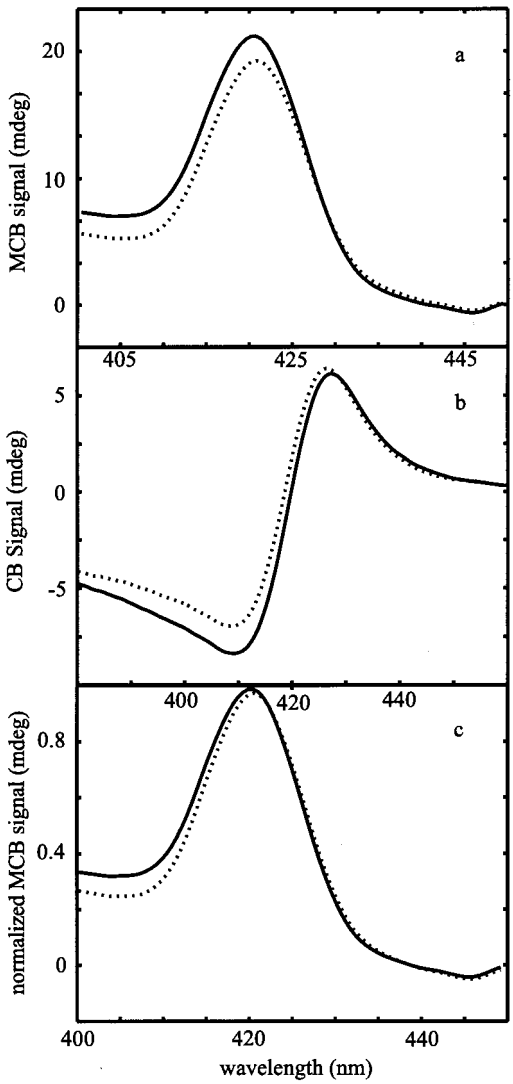

Figure 5. Effect of sample stability on the determination of MCB and CB from reversed-field measurements as modeled by concentration mismatch (CM) (see eqs 12 and 13 in text). No mismatch (—); CM, sample concentration 20% smaller in the parallel field configuration (- - -). (a) MCB. Observed spectrum is attenuated and distorted by addition of CB in CM case. (b) CB. Observed CM-case spectrum is attenuated and distorted by addition of MCB. (c) MCB from panel a normalized to maximum intensity demonstrates band shape distortion.

Optical Distortions. The following sections consider the effects of optical imperfections and artifacts on near-null polarimetric measurements (at a given field configuration). In general, the effects of these nonideal cases can be reduced to three empirical types: attenuations, offsets, and distortions of time dependence, as discussed further for the cases below.

Insensitivity to Strained Optics. An important advantage of the near-null MORD technique over the ellipsometric MCD method is that magnetic optical activity may be measured with much less sensitivity to interference from the linear birefringence that can be introduced by inadvertent strain present in optical components (or by sample photoselection, see below). Linear birefringence enters in first order to the expressions describing the ellipsometric CD signal,[19] whereas it enters only to second order in near-null ORD. Although this first-order LB signal may be subtracted out in MCD by taking the difference of opposed-field measurements, the second order coupling of LB with the Faraday rotation of solvent and cell, which can be relatively large, does not cancel between opposed-field MCD measurements. These particular LB artifacts do not appear in near-null ORD and MORD measurements. However, their LD analogues do appear in ORD and MORD and are considered below for the case of photoselection-induced LD in light absorbing samples.

Naturally occurring strain in optical cells or components may be difficult to characterize because it is often neither uniaxial nor uniform. Well-characterized strain may be obtained with a strain plate, e.g., a circular quartz plate compressed from the edges to produce a nearly uniaxial strain whose magnitude may be adjusted by varying the intensity of compression.[29] An adjustable strain plate with its fast axis rotated to various orientations, placed in front of the sample cell (outside the magnetic field), thus serves as a tractable model for the effect of a strained entrance window derived in paper 1 in this series.

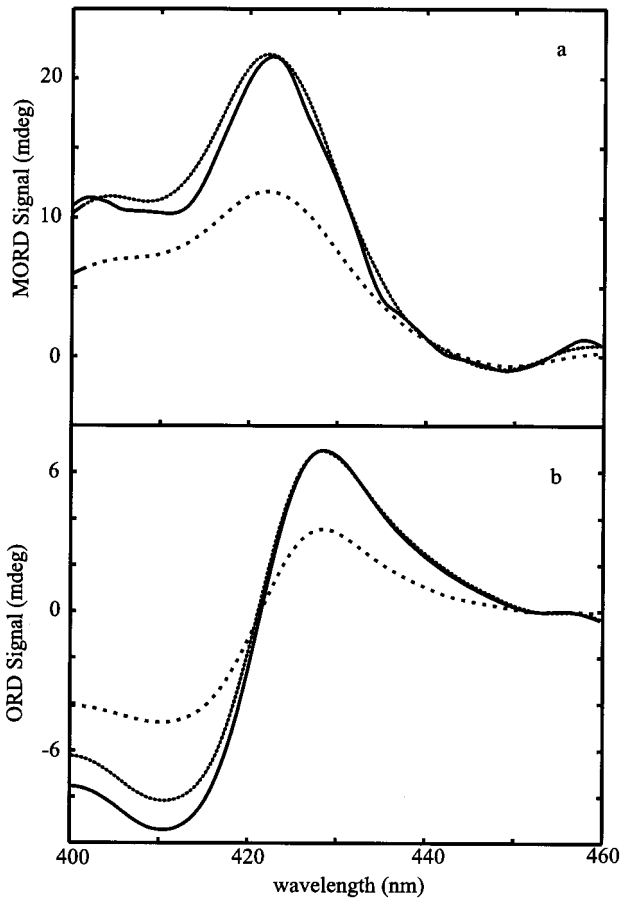

Figure 6. Effect of window strain on observed MCB (a) and CB (b). No strain (—); Case I (···), front window strain oriented at $\varphi = 45°$, shows maximum LD artifact; Case II (- - -), $\varphi = 0°$, shows minimum LD artifact. Strain magnitude, δ, is 3°. Data curves are offset several mdeg to facilitate comparison.

A maximum strain value of 2° (δ_1 at 425 nm) is used in the examples presented in Figure 6, a value that is large compared to strain levels typically tolerated in near-null measurements but comparable to levels found in commercial low-strain optical components.[30] Two limiting cases of the azimuthal angle are examined, $\phi_1 = 45°$ and 0° (cases I and II, respectively). For case I, the offsets are expected to be zero (preceding paper, eq 42) and the (wavelength dependent) attenuation is expected to be about 50% at 425 nm. The measured attenuation is 53%, and the offset is less than 3 mdeg. For case II, the (wavelength dependent) offset is expected to be proportional to δ_1 times the CD, or about 5% of the 425-nm signal, and attenuation is expected to be less than 1%. It is difficult to determine the attenuations and offsets with precision in this case because of the induced sample CD factor, but by minimizing the residuals between an attenuated combination of ideal CB and CD spectra and the measured signal, the amount of introduced CD and attenuation were determined to be within 8% of those expected from eq 42 in the preceding paper.

Imperfect Faraday Rotation. Equation 30 in the preceding paper describes the case in which the Faraday compensator does not exactly cancel the Faraday rotation of the solvent in both magnet configurations, producing an artifact that contributes in first order to the measured signal. Unlike previous cases, this artifact has a wavelength dependence that necessitates correction procedures to reduce spectral distortions that may interfere with the characterization of intermediates. In some cases, it may be possible to fit a polynomial baseline to an artifactual signal in spectral regions where the sample is known to have negligible MORD or ORD and extrapolate this baseline to a spectral region exhibiting optical activity for subtraction from rotatory data as a correction procedure.

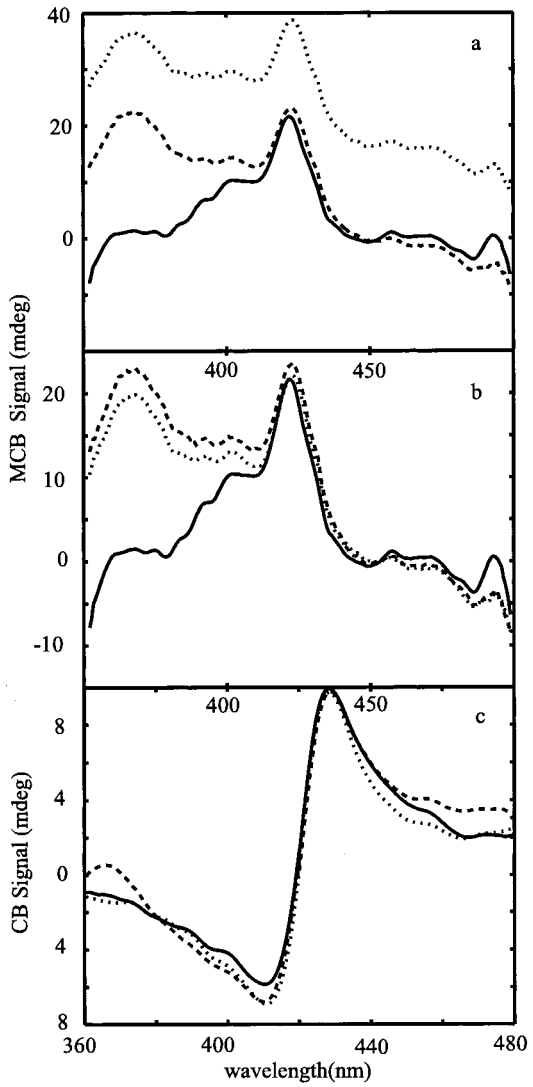

Figure 7. Effect of imperfect Faraday compensation. No mismatch between sample and compensator fields (both 1.00 T) (—); magnetic field of (matched cell) Faraday compensator increased to 1.03 T (···); matched-cell compensator replaced by glass plate of equal length in 1.00 T field (- - -). (a) Measured MCB signal. (b) Measured MCB after subtracting an offset of the signal at 450 nm to zero. (c) Measured CB signal. Note that panels a and b are plotted over a larger wavelength region than c.

Two nonideal cases demonstrating the effect of improper Faraday correction were investigated: (1) the magnetic field at the compensating matched cell was increased to 1.03 T in the parallel configuration and (2) the Faraday rotation of a 10-mm glass plate was used to balance the Faraday rotation of a quartz cell and water solvent. The latter case demonstrates the (time independent) distortion caused by using an unsuitable material for the Faraday compensator. In this case, although the wavelength-averaged Faraday rotation was canceled by the mismatched compensator, substantial wavelength dependence is introduced into the spectra because the Faraday effect for the compensator and solvent have different dispersions. This is shown in Figure 7. As expected from paper 1 of this series, eq 30, the major effect seen for both cases is the introduction of a field-dependent birefringent offset to MCB signal and no

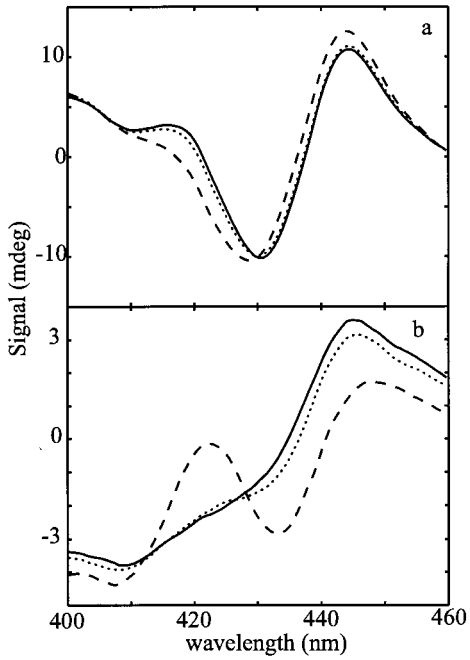

Figure 8. Measured MCB (a) and CB (b) after photolysis of MbCO at $\rho = 0°$ (—), 5° (•••), 10° (- - -) in the presence of a small misalignment (ca. 1°) from zero in the angle χ. Note that the $\rho = 0°$ excitation geometry shows minimum sensitivity to variations in χ and ρ. See Figure 9 for angle definitions.

net offset to the determined CB. The apparent attenuations are small, about 1%, as expected.

Photoselection-Induced Orientation. Oriented samples, such as photoselected solutes, can exhibit a linear dichroism that will contribute in first order to near-null ORD measurements (paper 1 in this series, eq 25). This section demonstrates the expressions in paper 1 of this series predicting the effects associated with partial orientation by photoselection, as such orientation introduces both offsets and attenuations that depend on the orientation of the sample's linear dichroism. The detailed analysis presented there predicts a coupling between the linear dichroism of the sample and the Faraday rotation of the solvent. This coupling has a different dependence on photoselection geometry than the first-order linear dichroism term (preceding paper, eq 46). This coupling can be quite large because of the relatively large size of the Faraday effect of the solvent and cell windows, which is typically on the order of degrees. Hence, an excitation geometry that minimizes the contribution of linear dichroism to the measured signal may actually maximize the contribution of the coupling to the detected signal. Empirical confirmation of this coupling is a focus of this section. It also demonstrates that by probing along the unique axis of the photoexcited sample, the sample appears to be isotropic and oriented sample terms vanish. This geometry should also be insensitive to alignment errors to first order,[31] as demonstrated in Figure 8. An excitation geometry that achieves this isotropic excitation has an excitation pulse propagating at 90° to the probe propagation direction and is polarized parallel to the probe propagation.[32]

The distribution of excited molecular orientations with respect to the probe-source polarization was controlled by changing χ and ρ, angles illustrated in Figure 9. Here, χ is zero for LP1 polarized along the *X* axis. Setting the laser polarization parallel ($\rho = 0°$) or perpendicular ($\rho = 90°$) to the probe propagation direction corresponds, respectively, to the crossed parallel and crossed perpendicular geometries described in paper 1 of this

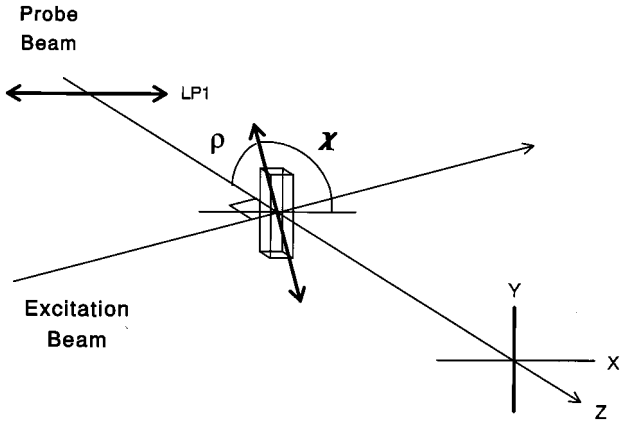

Figure 9. Schematic illustration of some orientation angles for devices and light beams in laser-photolysis near-null polarimetric MORD apparatus. Magnetic-field lines (not shown) are parallel (or antiparallel) to the probe beam propagation vector (*Z* axis). The probe-beam propagation and polarization vectors (single- and double-headed arrows, respectively) define the *XZ* plane. The probe beam is shown after emerging from the first polarizer (LP1) with linear polarization along the *X* axis. The excitation beam is shown coming in from below the *XZ* plane, and ρ is the polarization angle of the excitation laser with respect to the *Z* axis. Crossed (90°) beam excitation is shown with the excitation polarization vector perpendicular to the probe-beam propagation ($\rho = 90°$). The photoselection axis in this case has an azimuthal angle of χ if the laser propagates at an angle $\chi - 90°$ to the *XZ* plane. (Another excitation geometry discussed in the text is crossed beam with excitation laser polarization parallel to probe propagation, i.e., $\rho = 0°$.)

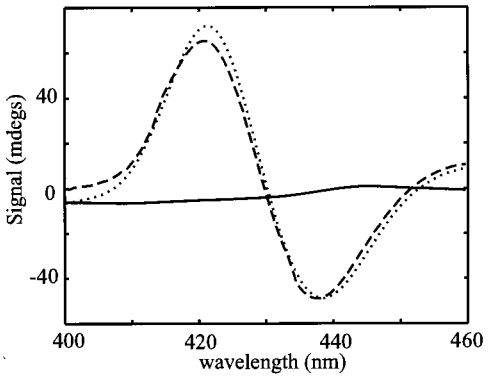

Figure 10. Sensitivity of near-null natural optical rotation measurements to linear dichroism artifact at 1 μs after laser photolysis of MbCO in glycerol/water. The signal measured at $\chi = 0°$ (—) corresponds to CB. Normalized absorption difference spectrum for the same sample represents the LD band shape (•••). The signal measured at $\chi = 20°$ (- - -) contains both CB and LD.

series. For an excitation geometry with χ equal to 0° and ρ equal to 90°, the expected LD contribution is zero and the contribution from the coupling term is maximized (preceding paper, eq 46). By simply rotating the polarization by 90° ($\rho = 0°$), the sample is probed along the unique axis and appears to be isotropic, eliminating the contributions of linear terms.

Figure 10 demonstrates the introduction of LD terms into the time-resolved optical rotation signal of photolyzed MbCO, here dissolved in glycerol/water solvent in order to extend the rotational diffusion time constant, as the excitation polarization orientation deviates from the probe polarization, i.e., $\chi \neq 0$. As predicted from paper 1 in this series, eq 46, χ rotation (20°) introduces a (first order) negative LD term to the measured signal. The LD term introduced resembles the inverse of the transient-absorption spectrum, as measured on a time-resolved optical absorption instrument (differences are attributable to the

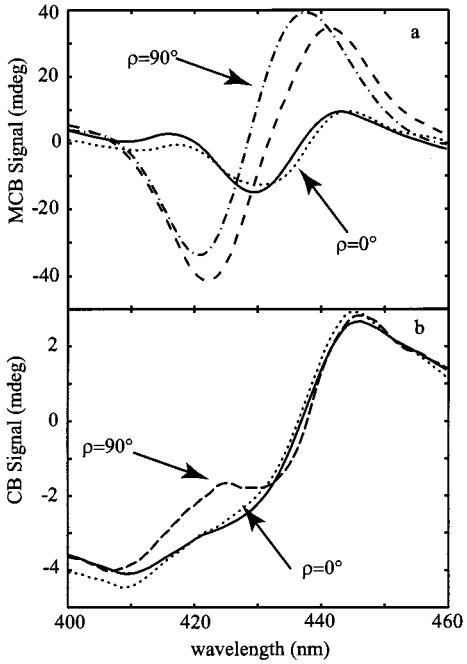

Figure 11. Effect of orientation by photoselection on MCB and CB measurements at 1 μs after photolysis of MbCO in viscous glycerol/water solvent at $\chi = 0°$. (a) Observed MCB signal. $\rho = 0°$: glycerol (···); no glycerol (—). $\rho = 90°$: glycerol (-·-); normalized 1-μs absorption difference spectrum (- - -) corresponding to band shape of LD artifact. (b) Observed CB. $\rho = 0°$: glycerol (···); no glycerol (—). $\rho = 90°$, glycerol (- - -). The close agreement between measurements made at $\rho = 0$ for viscous and nonviscous solvent demonstrate that this geometry is least sensitive to LD artifacts arising from photoselection-induced orientation.

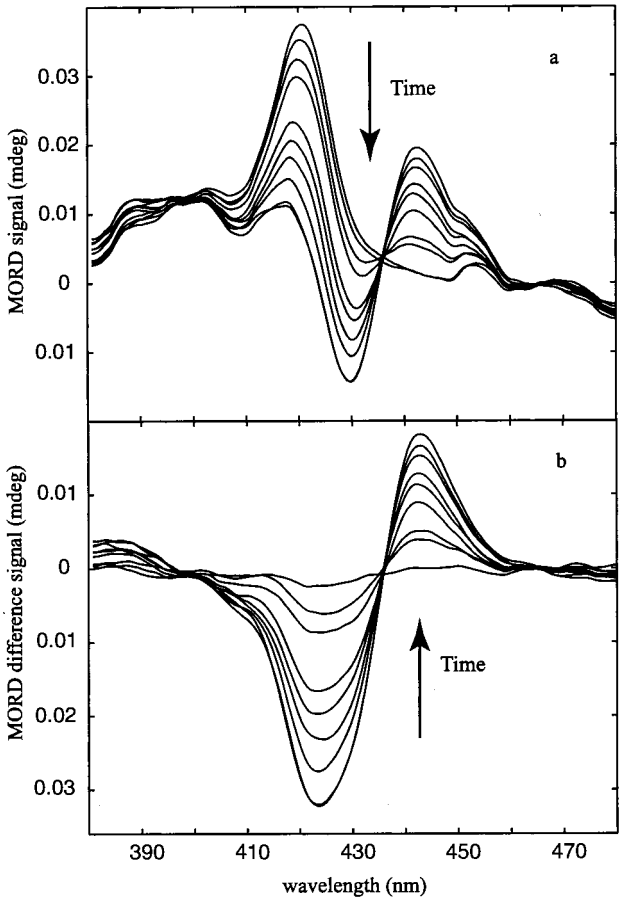

Figure 12. Absolute Soret TRMORD spectra and difference (transient − prephotolysis) spectra after laser photolysis of MbCO, collected at logarithmic time intervals: 10, 22, 46, 100, ..., 10000 μs.

presence of optical rotation in the signal). Because the sign of the (second order) Faraday-LD coupling term varies with the sign of the field and CB was determined from the sum of opposed-field measurements, it does not contribute to the LD artifact in this case (see discussion below). This example shows that a modest deviation in angle from 90° introduces a large LD component due to the disparity in size between linear dichroism and optical rotation.

Figure 11a demonstrates the introduction into the time-resolved MCB signal of an artifact corresponding to the coupling between the solvent−cell Faraday rotation and the photoselection-induced linear dichroism of the sample (MbCO in glycerol/water). The MCB signal measured for an excitation geometry of $\rho = 0°$ (artifact free) is compared to a geometry of $\rho = 90°$ exhibiting the coupling term ($\chi = 0°$ in both geometries). The prediction of such a coupling effect follows from the Mueller analysis presented in the preceding paper. It may also be understood intuitively by considering the apparent change in LD azimuthal angle that the probe beam experiences as its polarization angle undergoes Faraday rotation within the sample; this apparent azimuth determines, in turn, how much additional rotation the LD will itself contribute to the beam's polarization. The optical absorption of the sample taken at the same time is shown to demonstrate that the spectral profile of the induced term is determined mainly by the linear dichroism, although the relatively featureless dispersion of the solvent−cell optical rotation will also be convoluted into this term. The same panel shows that when probed along the unique axis ($\rho = 0°$), the sample appears to be isotropic by symmetry and the coupling is zero. The MCB of the same sample in water, where fast rotational diffusion results in an isotropic sample at the time of measurement, is shown for comparison. (Small disagreements are due to differences in photolysis levels and cell composition and to spectral changes associated with solvent composition.)

Figure 11b shows the effects of the above excitation geometries on the natural CB obtained from reverse-field measurements. The $\rho = 0°$ case agrees well with the measured signal in water. For $\rho = 90°$, a small LD signal is present. This is attributed to small misalignment in the angle χ from its nominal value of zero in this example, highlighting the fact that even small errors can have a pronounced effect on the CB for $\rho = 90°$. It should also be emphasized that this geometry is impractical for MCB measurements because of the coupling term and is discussed here to emphasize the sensitivity of this particular geometry to angular misalignment. Figure 8 illustrates the relative insensitivity to angular misalignment of the $\rho = 0°$ case; several degrees of angular misrotation are required to introduce distortion into the MCB or CB reverse-field measurements. The CB term is more sensitive in this case to these angular misalignments than the MCB term because of its smaller size.

TRMORD and TRORD of Photolyzed MbCO. The difference (transient − prephotolysis) TRMORD spectra in Soret bands are shown in Figure 12, and the corresponding TRORD bands are shown in Figure 13. The TRMORD and the TRORD data (a total of 3072 wavelength scans per time point) were analyzed using SVD and global analysis. The signal-to-noise ratio of these data is about 100. Exponential fitting of the time-resolved MORD and ORD data gave an observed exponential decay time of 1.5 ms (standard deviation 0.1 ms). Time-resolved absorption measurements on the same sample (data not shown) yielded an identical lifetime, which is also similar

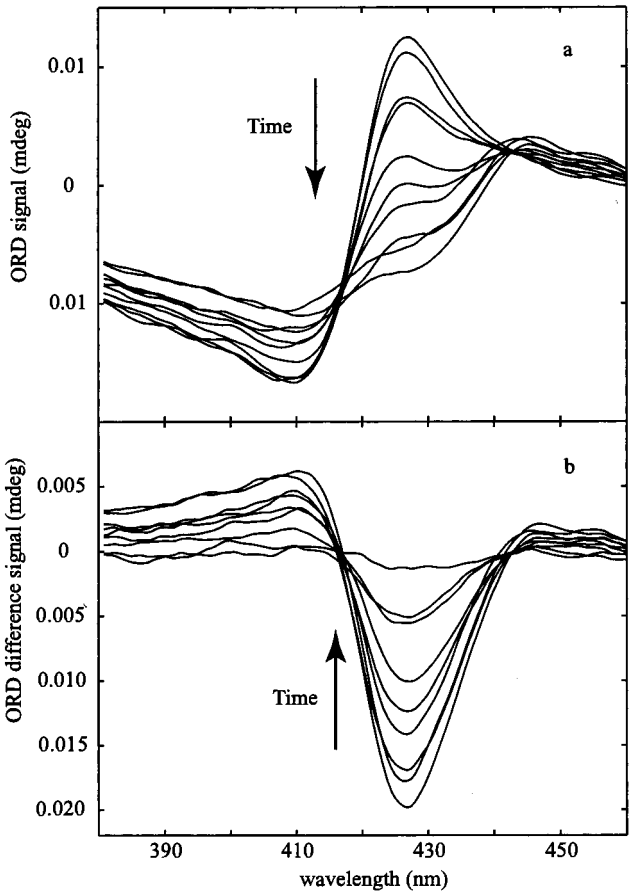

Figure 13. Soret TRORD spectra and difference (transient − prephotolysis) spectra after laser photolysis of MbCO, times given in Figure 12 caption.

to those previously reported for transient Soret absorption measurements in sperm whale (SW)[24] and horse[33] myoglobins.

The spectral changes associated in both MORD and ORD with this lifetime are consistent with those expected from ligand recombination, being nearly identical with the deoxy- minus carbonmonoxymyoglobin difference spectrum. Thus, the MORD and ORD results presented here agree with previous assignments of this rate to bimolecular recombination of CO to the photolyzed myoglobin species. Ultrafast transient-absorption spectroscopy has shown that a deoxy-like absorption spectrum occurs within hundreds of femtoseconds following photolysis,[34] a result that suggests that nearly all of the conformational differences between ligated and unligated myoglobin in the region of the protein near the heme relax on a subpicosecond time scale. Accordingly, the TRMORD spectra seen at the earliest nanosecond times presented here also appear to be very much deoxy-like.

A small fraction of the photolyzed MbCO molecules undergo a geminate recombination reaction that occurs on a 100 ns time scale.[24,33] It has also been shown that at temperatures below about 200 K, the kinetics of the geminate process are highly nonexponential.[25] This has been attributed to the existence of a hierarchy of nonequilibrium conformational substates from which photolysis and geminate rebinding occur,[35,36] so that the kinetics become more exponential as the temperature is increased and interconversions between substates become more rapid. Although the Soret TRMORD measurements presented here do not have the time resolution needed to detect the geminate process, a more detailed study using the time-resolved MORD technique to examine the nature of protein relaxations following ligand photolysis of carbonmonoxy Mb with greater time resolution will be presented elsewhere.

The results presented here primarily serve to demonstrate a new capability introduced by the development of this near-null TRMORD technique, the ability to accurately measure nanosecond time-resolved MORD (and natural ORD) spectra with a signal-to-noise ratio suitable for global kinetic analysis. We demonstrate that this method is less sensitive to optical artifacts than is the ellipsometric method for measuring TRMCD, so that K−K transformation of data from TRMORD measurements may offer a preferable way to obtain TRMCD spectra in the presence of birefringence from strained optics. It also offers signal-to-noise advantages in that time-resolved magnetic optical activity may be measured outside of absorption bands. With regard to the myoglobin example presented here, it is interesting to note that the spectral changes associated with ligand recombination are much more evident in MORD (Figures 1 and 12) than in absorption. This example thus reflects what is expected to be a general advantage for TRMORD spectroscopy: MORD spectra generally contain spectral features and sign information not available in ordinary absorption, so that in many instances MORD spectroscopy is able to reveal information about the coordination chemistry of heme complexes that is not available from simple absorption.[1−5] The TRMORD technique demonstrated here now brings these advantages to the characterization of rapid kinetic processes in magnetooptically active systems such as heme proteins.

Acknowledgment. We thank Dr. Eefei Chen for assistance with myoglobin preparations and Dr. Jim Lewis for invaluable technical assistance. This work was supported by the National Institutes of Health, and the National Institute of General Medical Sciences Grant No. GM38549. D.B.K.-S. also acknowledges the support of an NIH postdoctoral fellowship, HL08969.

References and Notes

(1) Piepho, S. B.; Schatz, P. N. *Group Theory in Spectroscopy with Applications to Magnetic Circular Dichroism*; Wiley: New York, 1983.
(2) Sutherland, J. C. In *The Porphyrins*; Dolphin, D., Ed.; Academic: New York, 1978; Vol. 1, Chapter 4.
(3) Dawson, J. H.; Dooley, D. M. In *Iron Porphyrins*; Lever, A. B. P., Gray, H. P., Eds.; VCH: New York, 1989; Part 3, Chapter 1.
(4) Dooley, D. M.; Dawson, J. H. *Coord. Chem. Rev.* **1984**, *60*, 1−66.
(5) Shashoua, V. E. *Nature (London)* **1964**, *203*, 972−973.
(6) Shashoua, V. E. *Methods Enzymol.* **1973**, *27*, 796−810.
(7) Moscowitz, A. *Adv. Chem. Phys.* **1962**, *4*, 67−112.
(8) Barron, L. D. *Molecular Light Scattering and Optical Activity*; Cambridge University: Cambridge, 1982; Chapters 1, 6−7.
(9) Jackson, J. D. *Classical Electrodynamics*, 2nd ed.; Wiley: New York, 1975; Chapter 7.
(10) Faraday, M. *Philos. Trans. R. Soc. London* **1846**, *136*, 1−62.
(11) Stephens, P. J. *Annu. Rev. Phys. Chem.* **1974**, *25*, 201−232.
(12) Michl, J.; Thulstrup, E. W. *Spectroscopy with Polarized Light*; VCH: New York, 1986; Chapter 1.
(13) Che, D.; Goldbeck, R. A.; Kliger, D. S. *J. Chem. Phys.* **1994**, *100*, 8602−8603.
(14) Goldbeck, R. A.; Che, D.; Kliger, D. S. *J. Chem. Phys.* **1996**, *104*, 6930−6937.
(15) Shapiro, D. B.; Goldbeck, R. A.; Che, D.; Esquerra, R. M.; Paquette, S. J.; Kliger, D. S. *Biophys. J.* **1995**, *68*, 326−334.
(16) Che, D.; Shapiro, D. B.; Esquerra, R. M.; Kliger, D. S. *Chem. Phys. Lett.* **1994**, *224*, 145−154.
(17) Goldbeck, R. A.; Dawes, T. D.; Milder, S. J.; Lewis, J. W.; Kliger, D. S. *Chem. Phys. Lett.* **1989**, *156*, 545−549.
(18) Goldbeck, R. A.; Dawes, T. D.; Einarsdóttir, Ó.; Woodruff, W. H.; Kliger, D. S. *Biophys. J.* **1991**, *66*, 125−134.
(19) Che, D.; Goldbeck, R. A.; McCauley, S. W.; Kliger, D. S. *J. Phys. Chem.* **1994**, *98*, 3601−3611.
(20) Goldbeck, R. A.; Kim-Shapiro, D. B.; Kliger, D. S. *Annu. Rev. Phys. Chem.* **1997**, *48*, 453−479.

(21) *Handbook of Chemical Physics*, 63rd ed.; CRC Press: Boca Baton, FL, 1993; D-240, F-92. The viscosity of a 90% (w/w) solution at 26 °C was estimated by extrapolation from the viscosity tabulated as a function of percent glycerol, using the viscosity temperature dependence of pure glycerol.

(22) Henry, E. R.; Hofrichter, J. *Methods Enzymol.* **1992**, *210*, 129−192.

(23) Goldbeck, R. A.; Kliger, D. S. *Methods Enzymol.* **1993**, *226*, 147−177.

(24) Henry, E. R.; Sommer, J. H.; Hofrichter, J.; Eaton, W. A. *J. Mol. Biol.* **1983**, *166*, 443−451.

(25) Vickery, L.; Nozawa, T.; Sauer, K. *J. Am. Chem. Soc.* **1976**, *98*, 343−350.

(26) Volkenstein, M. V.; Sharonov, J. A.; Shemelin, A. K. *Nature (London)* **1966**, *209*, 709−710.

(27) Note that the sign conventions used in MORD reports appearing in the early literature are often inconsistent with modern chemical usage.

(28) Samejima, T.; Kito, M. *J. Biochem.* **1968**, *65*, 759−766.

(29) Esquerra, R. M.; Lewis, J. W.; Kliger, D. S. *Rev. Sci. Instrum.* **1997**, *68*, 1372−1376.

(30) Strain in cell windows can be detected with more sensitivity using the ellipsometric CD method (see ref 31) than by visual inspection using crossed sheet polarizers, the method typically used by commercial suppliers of low-strain cells.

(31) Björling, S. C.; Goldbeck, R. A.; Milder, S. J.; Randall, C. E.; Lewis, J. W.; Kliger, D. S. *J. Phys. Chem.* **1991**, *95*, 4685−4694.

(32) Esquerra, R. M. Ph.D. Dissertation, University of California, Santa Cruz, 1997.

(33) Chen, E.; Kliger, D. S. *Inorg. Chim. Acta* **1996**, *242*, 146−158.

(34) Martin, J. L.; Migus, A.; Poyart, C.; Lecarpentier, Y.; Astier, R.; Antonetti, A. *Proc. Natl. Acad. Sci. U.S.A.* **1983**, *80*, 173−177.

(35) Austin, R. H.; Beeson, K. W.; Eisenstein, L.; Frauenfelder, H.; Gunsalus, I. C. *Biochemistry* **1975**, *14*, 5355−5373.

(36) Ansari, A.; Berendzen, J.; Bowne, S. F.; Frauenfelder, H.; Iben, I. E. T.; Sauke, T. B.; Shyamsunder, E.; Young, R. D. *Proc. Natl. Acad. Sci. U.S.A.* **1985**, *82*, 5000−5004.